Review Article

Matthias Cumme* and Arnaud Deparnay

From regular periodic micro-lens arrays to randomized continuous phase profiles

Abstract: Illumination systems for various industrial applications, e.g., in semiconductor industries and medical treatment techniques, require a specific and well-adapted intensity distribution with maximum efficiency, best achievable accuracy, and highest flexibility in the selection of the target light field. Additionally, for particular applications, all these aspects have to be fulfilled simultaneously for different wavelengths. In most of these situations, the challenging optical specifications are accompanied by the requirement of a cost-efficient fabrication technique, suitable at least for batch or small series production. In the present contribution, we first retrace the development steps and performance progress of micro-optical-based beam shaping setups. Secondly, we discuss the possibilities resulting from a combination of both refractive and diffractive optical characteristics. Especially, we show that a well-adapted combination of refractive and diffractive properties in a single element allows us to create achromatic diffusers with exceptional flexibility and high conversion efficiency.

Keywords: achromatic diffusers; micro-lens arrays; refractive diffusers.

OCIS codes: 140.3300; 230.1980; 230.3990.

DOI 10.1515/aot-2014-0062
Received November 20, 2014; accepted January 6, 2015

***Corresponding author: Matthias Cumme,** Department of Microstructured Optics, Carl Zeiss Jena GmbH, Carl Zeiss Promenade 10, 07745 Jena, Germany,
e-mail: matthias.cumme@zeiss.com
Arnaud Deparnay: Department of Microstructured Optics, Carl Zeiss Jena GmbH, Carl Zeiss Promenade 10, 07745 Jena, Germany

www.degruyter.com/aot

1 Introduction

Generation of specific intensity distributions for illumination systems is a standard topic in the field of micro-optics. In many applications, creation and control of specific intensity distributions is an essential task, especially when large illumination angles have to be addressed. In applications with restricted installation volume or in illumination systems for high-end imaging instruments, illumination angles with a numerical aperture (NA) ranging up to 0.6 and with required efficiencies nearly 100% are very usual.

Refractive micro-optical elements such as regular micro-lens arrays are very common in illumination systems and have been used for a long time [1]. Due to their refractive working principle, micro-lens systems offer very high efficiencies. Especially in illumination systems using light sources with a beam quality factor M^2>20 (e.g., excimer lasers, high-power diode lasers, LEDs), micro-lenses are the key elements for the highly accurate homogenization of the light distribution [2–6]. Due to their regular periodic structure, classical low-loss micro-lens systems with 100% fill factor are limited to producing exclusively rectangular or hexagonal intensity shapes. In contrast to the advantages of maximum efficiency and high homogeneity, these restrictions turn out to be an essential drawback when more complex angular distributions are needed.

Unlike the micro-lens arrays, diffractive micro-optical elements (DOEs), especially diffractive diffusers, can produce nearly all arbitrary intensity distributions. Commercially diffractive multilevel beam shaping elements show commonly efficiencies up to 80–90%. The homogeneity of the intensity profile generated by a diffractive optical element is often highly sensitive to any fabrication error which causes appearance of disturbing zero or higher diffraction orders. Some methods were developed to compensate the zero diffraction order by interference [7, 8] or to separate it outside the illuminated area [9]. The influence of the zero diffraction order on the homogeneity increases significantly, when the produced illumination NA increases. This effect may become a real show-stopper in many applications.

In the present contribution, we discuss the opportunities to combine the advantages of refractive elements, namely their high efficiency without contribution to zero or higher diffraction orders with the advantages of diffractive elements, especially the large domain of producible intensity profile shapes. To investigate these possibilities, the design complexity of micro-optical elements will be increased step by step from regular micro-lens arrays to random micro-lens arrays and at the end to fully statistic, continuous profiles with mixed refractive/diffractive properties.

2 Regular micro-lens arrays

In comparison to diffractive elements, micro-lens arrays show a higher efficiency and a high reliability for challenging applications such as laser homogenization in lithography illumination systems.

The classical homogenizer setup (known as a fly's eye homogenizer) consists of a Fourier lens and two regular micro-lens arrays in tandem configuration [the second micro-lens array (MLA) is placed in the focal plane of the first MLA] (Figure 1).

The effect of homogenization is achieved by superposing the sub-beams from each individual lens in the focal plane of the Fourier lens. The far field of a fly's eye homogenizer shows good uniformity with well-defined edges. Due to the specific fly's eye configuration, the far field distribution is not influenced by the angular distribution of the input beam. Normally, introducing MLAs in illumination systems will increase the total beam divergence. To minimize this effect, the divergence introduced by the micro-lenses must not exceed the input divergence too much. Therefore, in illumination optics with the need of a nearly collimated and homogeneous illumination beam, micro-lenses with a very small output divergence and, therewith, very large radius of curvature are required. Figure 2 shows the topographical measurements of such a micro-lens array that produces a divergence with an NA of 0.02 at λ=193 nm, fabricated using calcium fluoride (CaF_2). For the single lenslet, a radius of curvature of 4.67 mm and a sag of 2.23 µm were measured. The derived profile deviation from an ideal sphere was 0.2% rms (root mean square). The measurements were carried out by the use of a white-light interferometer (PLµ 2300; Sensofar-Tech, S.L., Terrassa, Spain).

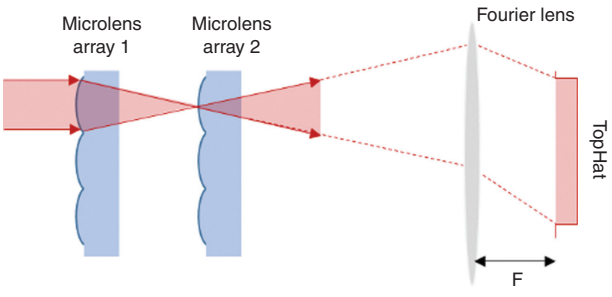

Figure 1 Principle of a fly's eye homogenizer.

Generally, the micro-optical elements that are discussed in the present contribution were produced using a typical lithographic structuring process that consists of:

- photoresist spin coating on a substrate,
- direct gray-scale laser beam writing,
- development, and
- ion beam etching for proportional transfer into glass.

Especially with direct gray-scale laser beam writing, it is possible to manufacture nearly arbitrary continuous surface relief profiles.

A fly's eye homogenizer with a double-sided micro-lens array eliminates the need for assembly and reduces the complexity of the homogenization system (see Figure 3). Our structuring technology allows a front to backside alignment with an accuracy of <0.5 µm. With the applied technology, a large number of different substrate materials can be processed [e.g., CaF_2, SiO_2, ultra low expansion glass (ULE), inorganic high index glasses], up to a maximum substrate thickness of 20 mm.

This manufacturing flexibility will be used to fabricate a double-sided homogenizer which is described in the following section.

In contrast to the advantage of high efficiency and homogeneity, homogenizers based on regular micro-lens arrays show a strong limitation in their flexibility of producing intensity profile shapes and illumination patterns. This limitation is caused by the imaging function of the system: the first micro-lenses act as apertures and their shapes will be imagined at the far field. Therefore, the feasible intensity shapes are given by the footprint shape of the micro-lenses. To achieve high efficiency during homogenizing and to avoid on-axis contributions that are not deflected and cause a zero-order-like intensity spot, the optical elements have to be structured with a fill factor of 100%. That means, only lens footprints fitting completely to each other can be used. A possible extension as compared to the rectangular lens structures discussed above that fulfill this constraint is a periodic hexagonal structure. If homogeneously illuminated circular areas are needed, such a hexagonal micro-lens array can be an alternative solution. However, also with the best fit of a circular area within a hexagon, an intensity loss of about 10% occurs.

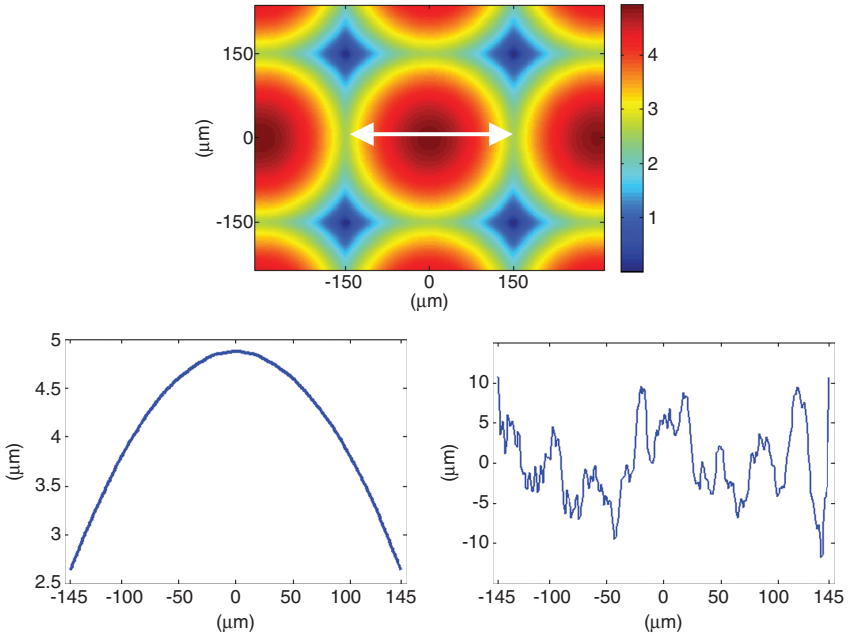

Figure 2 Top: White-light interferometry measurement of the topography of a micro-lens array in CaF_2. The pitch of the array is 300 µm. The color bar represents the height in µm. Bottom left: cross-section through an individual lenslet (corresponding to the double arrow from above). The sag height is 2.23 µm. Bottom right: deviation of the manufactured profile from an ideal sphere with a curvature radius of 4.67 mm. The profile deviation is 4.5 nm rms (=0.2% rms of sag).

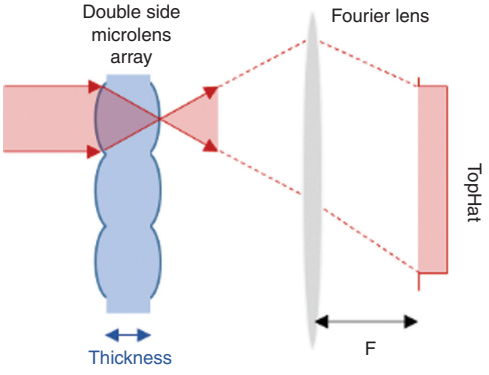

Figure 3 Principle of a fly's eye homogenizer using a double-sided micro-lens array.

Table 1 Parameters of the homogenization system.

Wavelength λ_w	980 nm
Input divergence	5°
Output divergence (x)	6.5°
Output divergence (y)	7.3°
Material	Fused silica ($n(\lambda_w)$=1.45)
Pitch	0.25 mm
Geometrical focal length of the arrays (in air)	2.5 mm
Optimized distance of the arrays in air Z_{arr}	2.1 mm
Corresponding thickness of the double-sided element ($n(\lambda_w)\cdot Z_{arr}$)	3.05 mm
Fourier lens focal length	1058 mm

3 Example: double-sided homogenizer

To demonstrate the working principle of a double-sided hexagonal micro-lens array-based homogenizer, a design for a high laser power application will be discussed. In this specific application, a 1 MW beam, which is produced by 164 000 laser diode emitters, has to be transformed into a homogeneous beam that in turn will be used as a pumping source for a circular CaF_2 laser crystal [10]. The specification of the discussed design is shown in Table 1.

For the wave optical simulation of the far field distribution, a source model consisting of 4000 single emitters was used because of the computing power limitation. The combined emitters produce an input beam of 100 mm diameter with a divergence of 2.8° in the x-direction and 5° in the y-direction. The resulting far field distribution is shown in Figure 4. The simulated efficiency of the hexagonal far field was 98%, and the simulated homogeneity ±3.5%. The maximum encircled disk in the hexagon comprises 89.3% of the total value. The homogenized far field intensity pattern shows a slope width of 14% of the overall divergence (Figure 4).

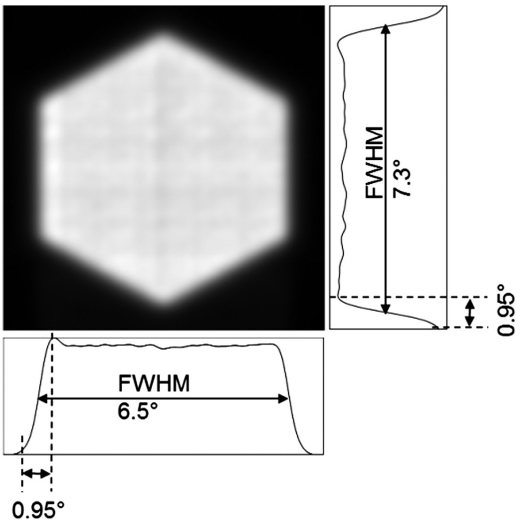

Figure 4 Simulated far field distribution using a wave optical source model consisting of 4000 single laser diode emitters. The asymmetries in the far field distribution are due to systematic cutoff effects in the computation (FWHM: Full width at half maximum).

In the basic configuration setup of an imaging fly's eye homogenizer, the second micro-lens array, which is equal to the first one, is positioned at the geometrical focal plane of the first array. Additionally, the focal point of the Fourier lens coincides with the focal plane of the first micro-lens array. In our case, due to the divergence of the input beam and also taking diffraction effects into account, which especially occur at the apertures of the micro-lenses, the homogenization task becomes more complex and the geometrical simplification of the basic setup has to be abandoned.

Therefore, in our wave-optical simulation we changed the geometrical parameters of the basic setup so that a maximum profile homogeneity with minimum disturbing diffraction effects occurs in the target field. Especially, we found an optimized distance of the lens arrays which was shorter than their geometrical focal length. This finding correlates with the more general observation that the peak irradiance derived from diffraction theory and the geometrical focal length shows a significant deviation for micro-lenses with small Fresnel numbers [11, 12]. Finally, the substrate thickness results from the optimized array distance in air Z_{arr} and its refractive index at the working wavelength $n(\lambda_w)$.

The calculated design was fabricated using direct gray-scale laser beam writing followed by a subsequent ion beam etching process. Figure 5 shows an interferogram of the surface of the fabricated lens array in fused silica.

The investigation of the optical function was done using a collimated white-light LED beam with a divergence of 3.6°. Figure 6 shows both the camera pictures of the incoming LED beam profile (left) and the homogenized output beam profile (right). The homogeneity of the homogenized output profile was measured to be within ±4% within the whole intensity distribution. Here, the homogeneity is defined by the ratio $(I_{max}\text{-}I_{min})/(I_{max}+I_{min})$ in the area between the two encircling maximum side lobes (see the intensity profile of Figure 6, lower right). I_{max} and I_{min} denote the maximum and minimum intensity, respectively.

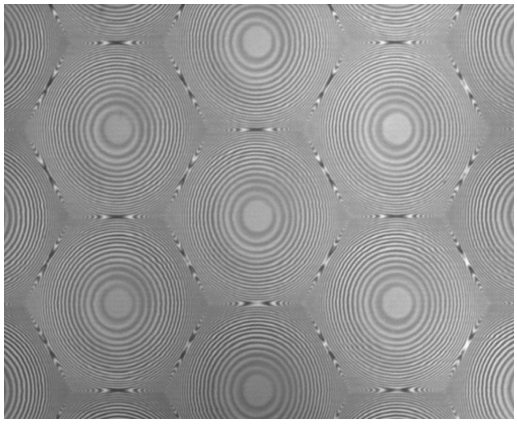

Figure 5 Interferogram of the fabricated hexagonal microlens array (material: fused silica, pitch 250 μm, sag 9.3 μm).

Resuming we can state that only a few different far field shapes (square, hexagonal, triangle, and lines) and distributions (top-hat) can be realized with high-efficiency close-packed regular spherical microlens arrays. Extension of design freedom, e.g., by using of aspherical or parabolic regular lenses, will lead to minor modifications of the optical function [13].

4 Random micro-lens arrays

To extend the spectrum of achievable intensity distributions, we turn from regular micro-lens arrays to laterally randomly distributed lenslets.

Such a randomly distributed micro-lens structure acts as a highly efficient diffuser which typically shows a Gaussian or a super-Gaussian intensity distribution. The main positive characteristics of these elements are their design flexibility, the low zero-order contribution, and the possibility of generating almost smooth and uniform intensity patterns. The broad design flexibility is geometrically constrained by the choice of the position of the individual lenslets, their sag height, and their radius of curvature.

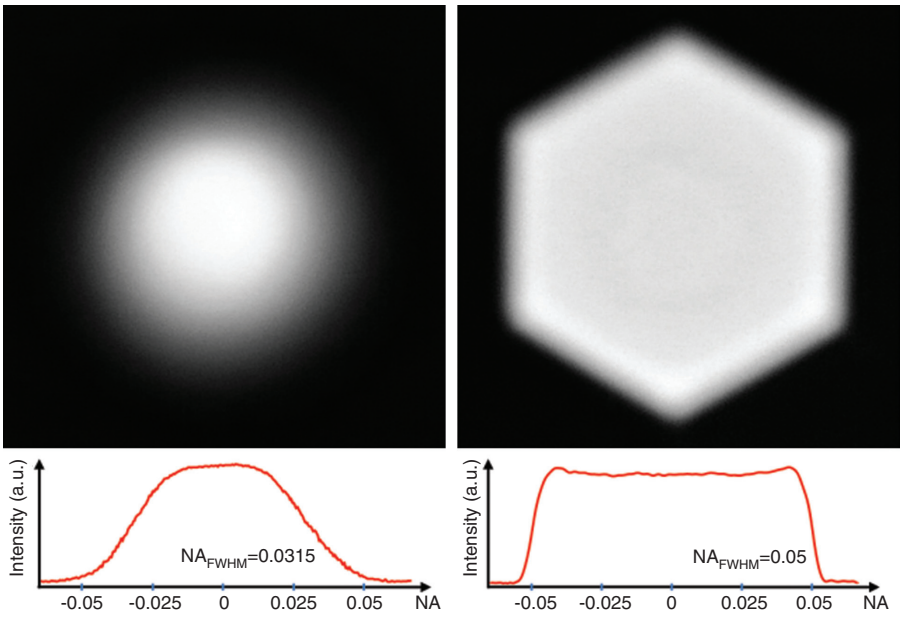

Figure 6 Left: measured intensity distribution of the input beam of a collimated white-light LED. Right: measured far field intensity distribution resulting from the double-sided hexagonal micro-lens array.

Using a coherent plane wave as an input source, such a diffuser will produce a fully randomized speckle far field intensity distribution. In comparison, using the same source, a conventional periodic micro-lens array will generate a regular array of diffraction spots in the far field.

When a partially coherent light source is applied, the far field distribution resulting from a regular micro-lens array may exhibit some disturbing periodic inhomogeneities. These perturbations occur when the pitch size of the array is not well adapted, especially when it is smaller than the spatial coherence length of the source. Using the same partially coherent light source, a random micro-lens array with similar typical lens sizes as the regular array shows a far field with non-periodic inhomogeneities, which have a smaller disturbing effect on illumination applications [14].

A simple method for the design of randomly distributed lenses is the use of a Voronoi tessellation [15, 16]. A set of starting positions, the future central lens positions, is randomly distributed over a surface (see the red dots in Figure 7). For each of these starting positions, an individual so-called Voronoi cell is defined as the region covering the area which is closer to this specific position than to any other (see the blue-rimmed cells in Figure 7).

Subsequently, each Voronoi cell is covered with a convex or a concave lens. Exemplarily, Figure 8 shows the topography of a convex randomly micro-lens array. Due to the unique property of the Voronoi tessellation and in order to avoid disturbing phase steps between two lenses,

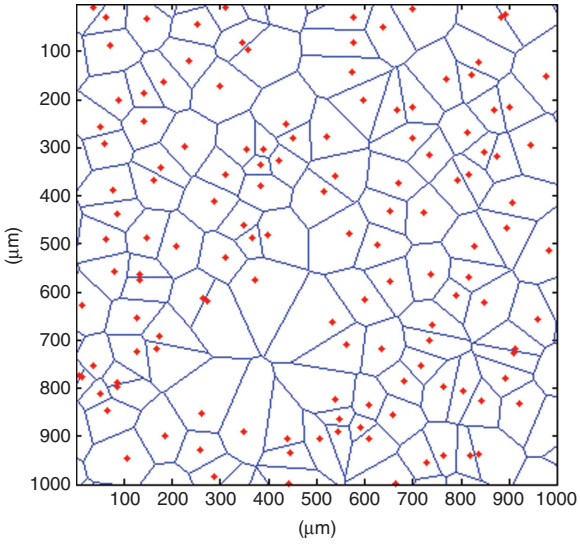

Figure 7 Voronoi tessellation: the red dots are statistically distributed starting positions. Each cell (blue encircled polygon) covers the area which is closer to the related specific starting point than to any other one.

all the micro-lenses must have the same radius of curvature. It is important to notice that the center positions or maximum sag heights of all lenslets are located in the same plane. Because a linear section through the randomly distributed two-dimensional lenslet pattern never hits all maximum positions, the cross-section through the height profile displayed in Figure 9 shows a variation in the maximum heights.

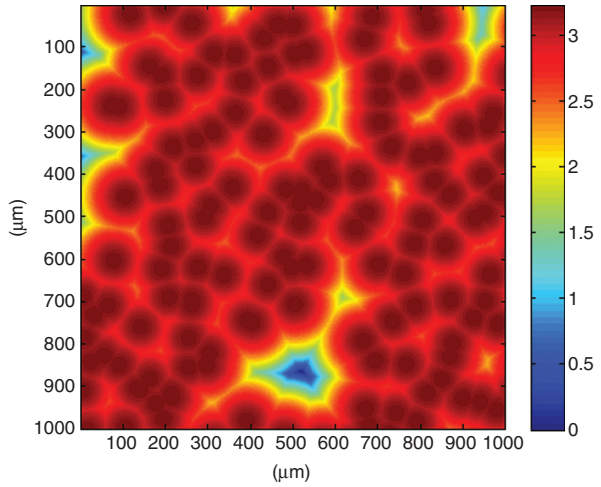

Figure 8 Filling up each Voronoi cell with a convex lens. All lenses have a radius of curvature of 4 mm. The color bar represents the profile height in µm.

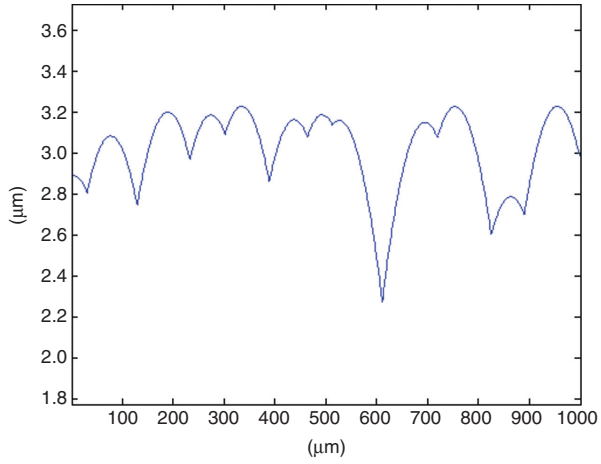

Figure 9 Cross-section of the randomly distributed microlenses. The lateral dimensions of the individual lenslet are in the range of hundreds of microns, their sag heights are measuring hundreds of nanometers.

At the far field, the superposition of all contributions from each individual lens generates a high-order super-Gaussian intensity distribution. The main drawback of this Voronoi tessellation-based design method is that the lens aperture sizes are not distributed completely evenly. Especially, the number of lenses with small apertures is too small. That means, intensity distributions with well-defined Gaussian shape cannot be achieved with this design method.

To overcome these limitations, we developed and implemented an extended design procedure, which we called the *iterative Voronoi calculation method* in analogy with the initial method.

The iterative method shows a possibility of designing a continuous random structure with rotationally symmetric micro-lenses. The design challenge is to get a continuous surface profile filled with convex microlenses without phase steps. The design comprises the following main steps:

- A plane surface 'Sd' at z=0 is selected and acts as the initial surface (Figure 10, left).
- A convex lens, defined by the spatial position of its center (x_c, y_c, z_c with z_c>0) and by its radius of curvature R, is plotted (Figure 10, center). All parameters (x_c, y_c, z_c, R) are selected randomly.
- The new surface envelops the maximum values of the overlaying originally surface with the sag of the convex lens (Figure 10, right).

In this manner, the plane surface is iteratively and continuously filled up with micro-lenses of various shapes. A white-light interferometer measurement of an element manufactured using this algorithm is shown in Figure 11.

In principle, the Gaussian far field distribution of a random micro-lens array based on the *iterative Voronoi calculation method* is characterized by the *central limit theorem* (see Figure 12). Hereby, it might be reasonable to assume that the areas covered by the individual lenslets are normally distributed and their contributions are also superposed in the same manner in the target plane. Design parameters (spatial positions of the lens centers, variety of focal lengths, of conic constants, and of aspheric coefficients) influence the Gaussian intensity distribution with a minor contribution.

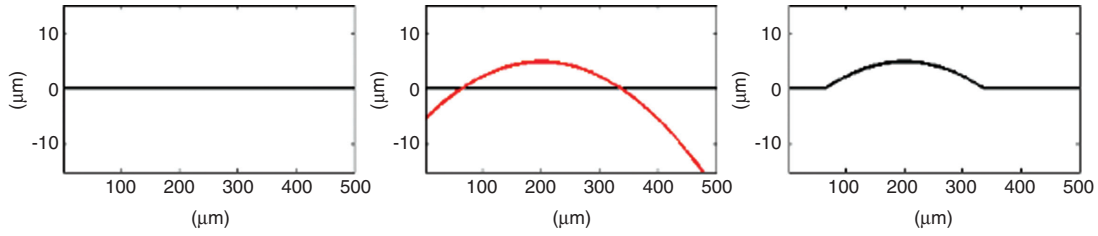

Figure 10 Principle of the *iterative Voronoi calculation method* (see the text for details).

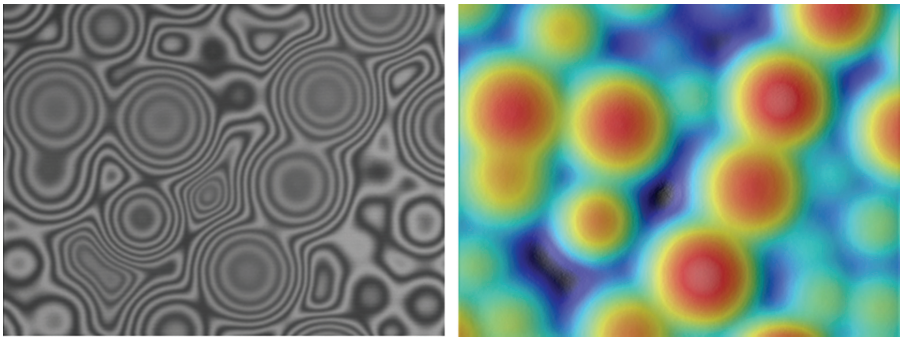

Figure 11 White-light measurement of a randomized microlens array designed by the *iterative Voronoi calculation method*. Left: interferogram, right: color-coded height profile (PLμ 2300, Sensofar). The displayed region covers an area of 250 μm×190 μm. The maximum height variation is 3 μm.

The *iterative Voronoi calculation method* enables the design of highly efficient, randomized micro-lens structures without any phase steps. The main drawback of this algorithm is its unidirectional calculation way. In comparison to the forward-backward applicable iterative Fourier transform algorithm (IFTA) [17], it is impossible to calculate a lens distribution for each specific arbitrary target far field distribution with this method. Random micro-lens structures are well suited, if Gaussian far field distributions have to be produced with high accuracy and efficiency. However, the unidirectional design algorithm shows restrictions in producing arbitrary intensity patterns and profiles.

5 Diffusers with continuous randomized profiles

As described in the previous section, the transition from regular lens arrays to randomly distributed lenses

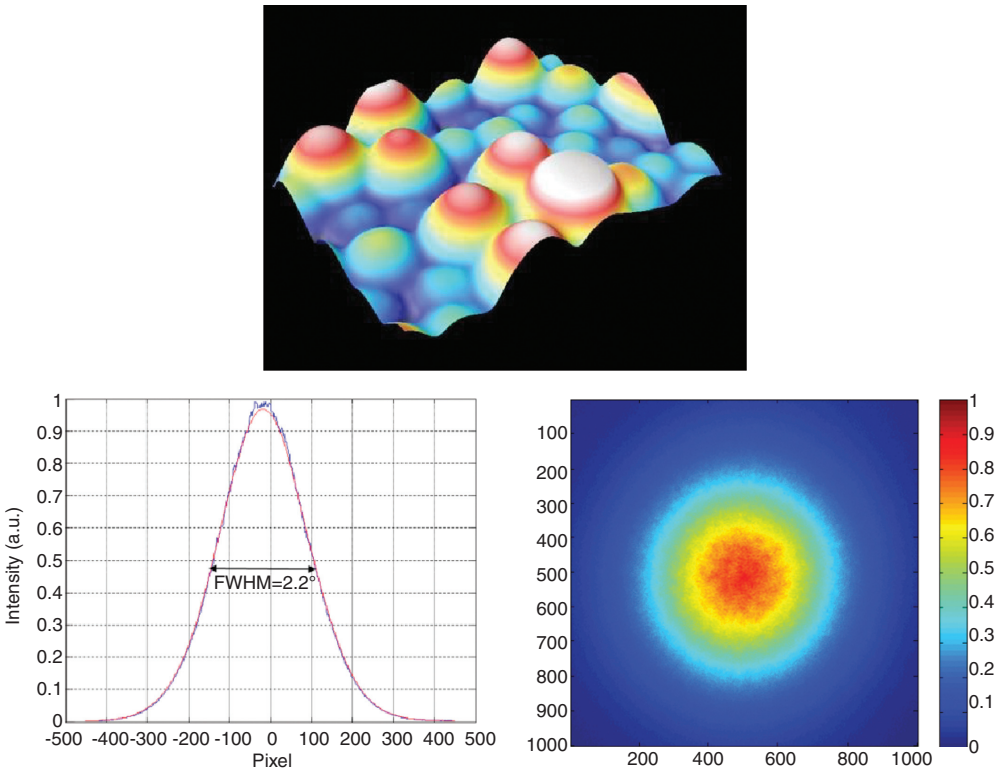

Figure 12 Far field distribution resulting from an array with randomly distributed microlenses which was designed by the *iterative Voronoi calculation method* at 193 nm (top: white-light interferometer topography measurement, bottom: far field measurement at 193 nm).

represents a solution that not only keeps the advantages of refractive micro lens systems (e.g., maximum efficiency, large-angle spectrum, and high degree of homogeneity) but also gives an extension of the intensity profiles that are producible (e.g., Gaussian and super-Gaussian instead of only top hats).

In spite of this extended variability, the generation of completely arbitrary, non-regular intensity distributions is not possible with randomized lens arrays because of their rotationally symmetric character [18].

Of course, to get a higher flexibility in the addressed angular spectrum of intensity, more freedom in the profile shape of the optical element is needed. Here, in principle, the traditional diffractive diffusers provide such 'high freedom' as arbitrary statistic element profiles and allow the shaping of nearly each arbitrary angular distribution [19]. Unfortunately, compared to the previously discussed refractive micro-lenses, diffractive elements also have significant disadvantages. Due to their diffractive character and also as a result of the usually used Fourier transformation-based design methods, the profiles of diffractive diffusers contain phase dislocations. Phase dislocations are points of discontinuity with a spiral shaped phase distribution. The alteration of the phase ϕ along a closed curve S encircling such a point is an integer multiple of 2π. Discontinuities as phase dislocations and 2π-jumps act as scattering centers which produce disturbing stray light and limit the achievable efficiency. Another important consequence is that phase profiles with spiral phase dislocations cannot be transferred into continuous profiles by phase unwrapping to overcome their drawbacks.

However, following the idea of the transition from regular micro-lenses to non-regular lens shapes, an interesting further step is leading to more or fully randomized structures which exhibit no phase discontinuity [20, 21]. This approach, on the one hand, will allow an extension of the application potentials and, on the other hand, it will keep all advantages of lens like continuous structures discussed before. For this purpose, a calculation method has been developed, which avoids the above-mentioned occurrence of phase dislocations at the very onset.

The design algorithm developed includes an optimization procedure for a merit function. It implies manufacturing aspects such as lateral resolution limits of the structuring process and the maximum achievable profile depth.

To fulfill all demands, a modified IFTA was developed that is comparable with the algorithm described in [20]. However, the algorithm described in [20] was applied to form only high-order super-Gaussian profiles. In most cases, IFTAs use a 2π-modulo phase representation that enables or encourages the occurrence of phase dislocations. To avoid phase dislocations at all, an IFTA-based design algorithm was developed which uses a non-modulo, biunique phase representation for producing arbitrary intensity profiles.

The fabrication of the continuous randomized design was done by direct laser beam writing. As the lateral resolution of the laser beam writer is in the order of 1 µm and the efficiently producible maximum profile depth is about 10–20 µm, a spatial frequency filter and a profile-height limitation procedure were implemented into the design algorithm corresponding to the manufacturing limitations.

To demonstrate the performance and test the potential of the continuous phase design algorithm, a non-symmetric seven-ray star target intensity distribution with a bright-dark contrast of 100% was chosen. The required NA of the distribution was 0.2 (=23° FWHM).

For comparison of the continuous design approach with the conventional diffractive design, we applied a classical IFTA and the modified IFTA for continuous phase distributions to find the same target distribution. The left side of Figure 13 shows a section of the conventional diffractive design. The expected phase dislocations are visible. The diffractive design was made for a target wavelength of 633 nm. For the simulated far field intensity distribution, which is depicted in Figure 14, an incoming laser beam with 2.5 mrad divergence (FWHM) was assumed. For the classical design approach, an intensity contrast of about 1:30 was reached at the design wavelength. Changing the wavelength leads to the well-known occurrence of the zero-order peak, which is caused by a phase shift mismatch at the positions of the 2π steps. Exemplarily, in the case of an illumination wavelength of

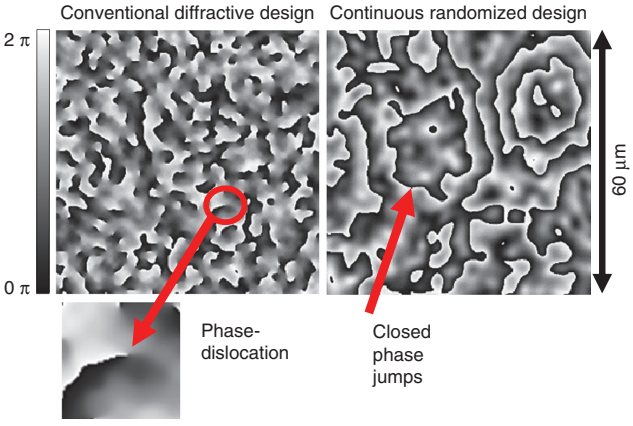

Figure 13 Section of a conventional diffractive design (left) and of a continuous randomized design (right).

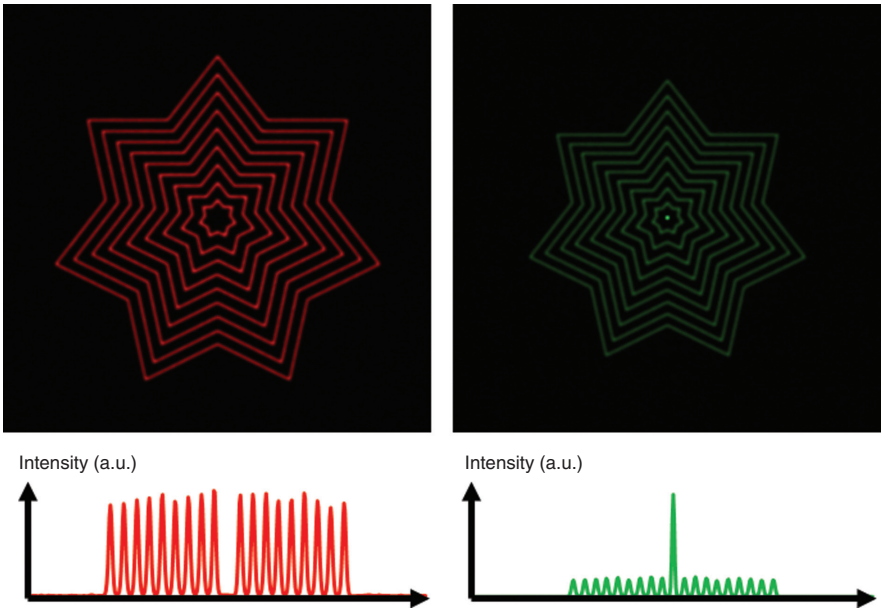

Figure 14 Simulated far field intensity distribution of the conventional diffractive design for two wavelengths (left: 633 nm, right: 543 nm with a zero-order peak).

543 nm, the simulation shows a zero-order share of 3.3%. With the 2.5 mrad incoming divergence, a ratio between the zero-order intensity and the target intensity of 5/1 was detected, which has a significant disturbing influence on the final intensity distribution (Figure 14, right).

The ratio of the zero-order intensity to the integrated intensity of the target distribution increases in a quadratic way with decreasing incoming divergence. Specifically, the ratio measures 30/1 for an incoming divergence of 1 mrad. Usually, due to fabrication imperfectness which leads to profile height and duty cycle errors, diffractive diffusers, fabricated by state-of-the-art methods, have a typical zero-order efficiency which is larger than 0.1–0.5%, depending on the structure size and NA. In the case of a large illumination NA, the zero-order contribution is also influenced by rigorous diffraction effects. The minimization of the zero-order contribution becomes even more difficult when the diffuser shows a wide structure size spectrum [8].

The right side of Figure 13 shows a part of the calculated continuous phase design in a 2π-modulo representation. The design was made also for a target wavelength of λ=633 nm. At the design wavelength, no disturbing zero-order peak was detected in the simulated far field intensity distribution. The simulated bright-dark intensity contrast of the produced intensity distribution was 1:17. In comparison to the classical diffractive design, the continuous design shows no phase dislocations. Therefore, in the 2π-modulo representation of the designed phase only closed 2π-steps occur (Figure 13, right). In contrast to diffractive profiles with spiral-shaped dislocations, such phase distributions can be unwrapped.

After unwrapping, the calculated phase profile was transferred into a height profile and fabricated by using direct laser beam writing. The measured surface profile is depicted in Figure 15 (top), and a cross-section of the profile is shown in Figure 15 (bottom).

The maximum profile depth of the manufactured element was about 10 µm. The measured intensity distributions using HeNe lasers with both 633 nm and 543 nm are shown in Figure 16. The measured NA of the star-shaped distribution was 0.2, which is close to the target value. The camera pictures show that the intensity contrast decreases with increasing angle. At the center, the contrast was measured to 1/2.5. At the largest angle, the contrast decreases to a value of 1/1. The measurement result can be explained with the resolution limitation of the laser writing system.

The fabricated profile shape can be regarded as a convolution of the target distribution and the writing resolution function. The convolution smears the small structure details, which are responsible both for the intensities propagating to the large angles and also for the high contrast. To produce large angles, either deep profiles with large profile gradients or small structure sizes are needed.

Despite the discussed profile aberration of the micro-optical element, the realized intensity distribution shows

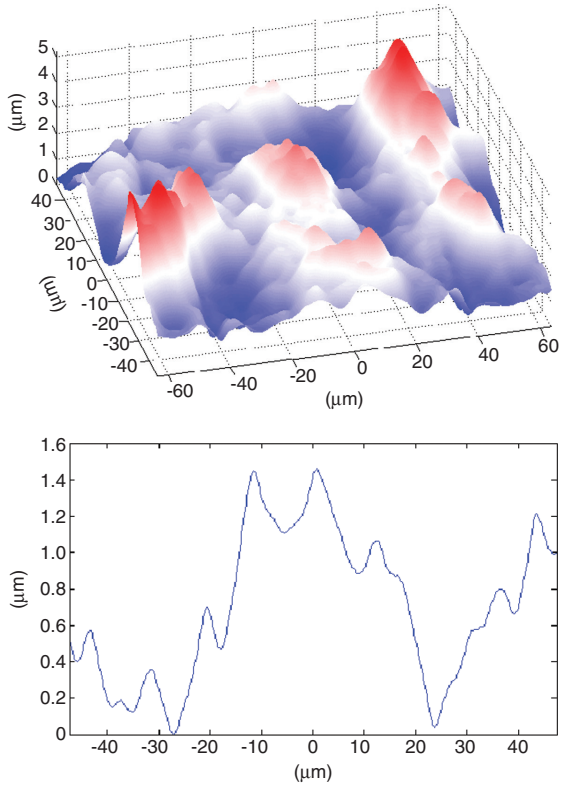

Figure 15 Measured height profile of the fabricated element with the continuous randomized design (top: 3D representation, bottom: a cross-section).

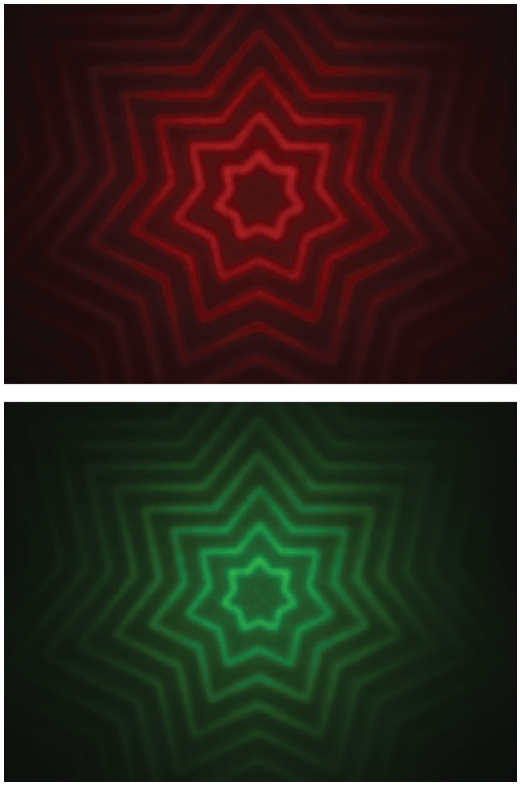

Figure 16 Measured far field intensity distributions of the fabricated element with the continuous randomized design for two wavelengths (top: 633 nm, bottom: 543 nm).

no zero-order contribution at the target wavelength of 633 nm. By changing the illumination wavelength to 543 nm, the measured intensity still shows no zero-order contribution. This measurement result at 543 nm impressively demonstrates the robustness of the design principle to wavelength changes or profile aberrations of the element structure. The main reason of this effect is the absence of 2π-phase steps in the design.

Additionally, comparing the sizes of the angular distributions at different wavelengths leads to the following interesting result. Both the measured intensity distributions at 633 nm and at 543 nm were added.

Figure 17 shows the resulting intensity pattern. Obviously the red color distribution shows a larger divergence in comparison to the green one. Measuring the ratio of angles for 633 nm/543 nm gives a value of 1/0.84. Taking into account the grating equation for a simple diffractive grating that produces a first diffraction order at the same angle, the angle ratio is 1/0.857 for the same wavelength change. Taking into account the measurement error, these two ratios are in the same order of magnitude. That means, the manufactured element acts much more as a diffractive element than as a refractive.

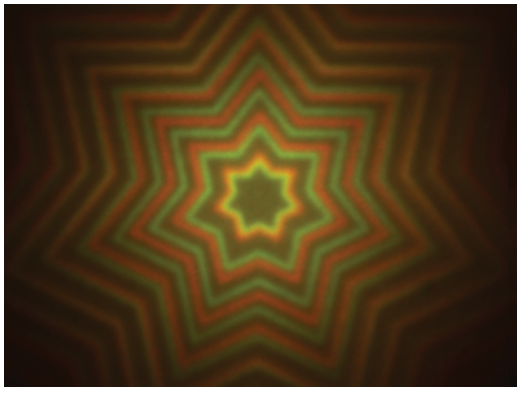

Figure 17 Summation of both measured intensity distributions at 633 nm and 543 nm.

6 Achromatic diffusers with a continuous phase profile

It is difficult to classify a completely randomized continuous phase structure as a pure ‘diffractive’ or ‘refractive’ micro-optical element. As discussed in the

previous section, the diffractive character of a micro-optical element will dominate when the majority of structure details are 'small', or more specific, when their dimensions are in the range of the working wavelength. In contrast, when the structure details are much larger than the applied wavelength, the micro-optical element will mainly show a refractive character. Generally, a preselected target intensity distribution can be achieved both by diffractive or refractive beam processing. This implies that a fine tuning of the dimensions of the element structure details of a randomized continuous phase element will allow adjusting a well-balanced compromise between refractive and diffractive contributions. Due to the inversed dispersion characteristics of the refractive and diffractive optical elements, a combination of both functionalities in a single element offers the opportunity for achromatization. This means, the intensity distribution in the far field is identical for two completely different wavelengths.

Systems that combine the diffractive and refractive optical effect in order to get an achromatic behavior were disclosed in several previous contributions (e.g., [22, 23]).

In the cited contributions, the achromatization effect was realized by the use of combined diffractive/refractive and diffractive/diffractive surfaces as a hybrid system. However, Fresnel losses, scattering effects, and parasitic orders produced by the diffractive elements lead to a limitation of the efficiency that can be reached by such hybrid systems. For example, the setup defined by two diffractive lenses with four phase levels used in reference [23] provides only a diffraction efficiency of 65%. In contrast to hybrid systems, the achromatization effect of the continuous phase diffuser discussed here is based on the diffractive/refractive behavior of a single optical surface instead of an element combination. Additionally, the diffractive part of the optical function is realized by a continuous profile structure without phase continuities. Therefore, the optical efficiency can reach nearly 100% for this approach in theory.

To test this design approach, a profile scaling procedure was introduced into the design algorithm which allows an adaption of refractive and diffractive contributions in a randomized continuous phase profile. The algorithm was tested with a ring-shaped target intensity distribution, which is shown schematically in Figure 18. The target divergence angle of the ring structure from center to center was 50 mrad (Figure 18).

For comparison, in addition to the achromatic design with a continuous phase profile, a conventional diffractive approach was also calculated. The design wavelength was set to be 555 nm.

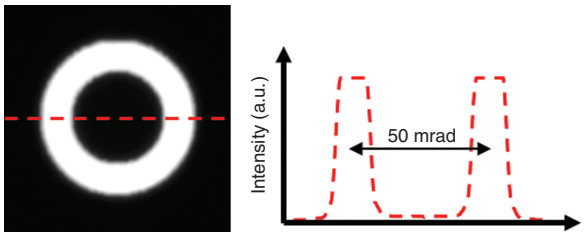

Figure 18 Target intensity distribution.

A section of the calculated profile is depicted in Figure 19. Figure 20 shows the simulated far field intensity distributions for the conventional diffractive design at different wavelengths. At the design wavelength, no zero-order contribution occurs. Changing the wavelength to smaller or larger values results in an increasing zero-order contribution and also changes the diameter of the produced ring intensity distribution. On the right of Figure 20 the added sum of the intensity profiles at 480 nm, 555 nm, and 630 nm wavelengths is depicted. This intensity sum exhibits a significant color fringe effect in which the outer part is dominated by red color and the central part by blue color. Figure 20 (bottom) shows the intensity profile variation by the wavelength change.

In comparison to the chromatic aberration of the diffractive design, the continuous phase calculation method with the profile size scaling procedure for achromatization shows a completely different property.

A section of the calculated achromatic phase element profile is shown in Figure 21. The theoretical efficiency of

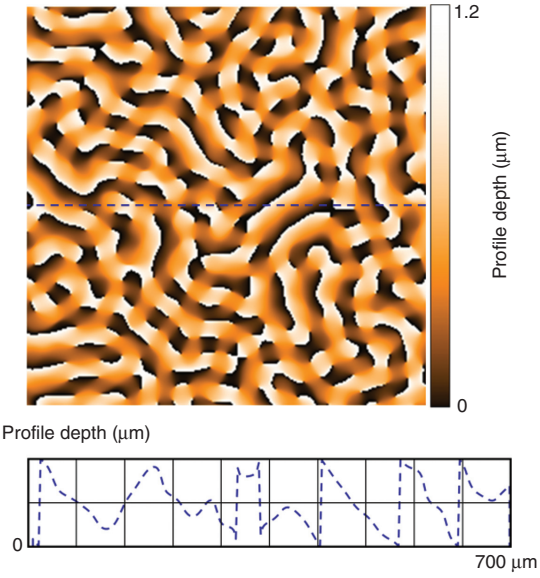

Figure 19 Height profile of the diffractive element.

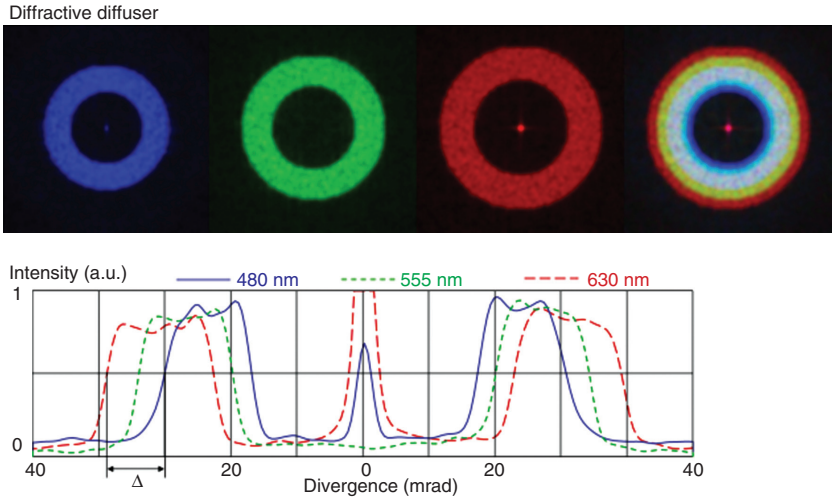

Figure 20 Top: simulated far field intensity distributions of a diffractive element at 480 nm, 555 nm, 630 nm (from left to right). The last ring on the right is the addition of the RGB colors. Bottom: cross-section of simulated intensity distributions.

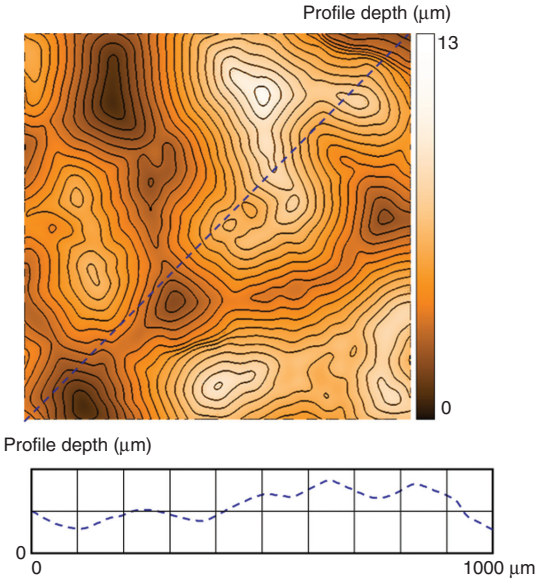

Figure 21 Height profile of the continuous randomized element.

the calculated achromatic ring shaping diffuser provides a conversion efficiency of 95%. The simulated far field distribution of the achromatic design is shown in Figure 22.

The three ring structures for the individual wavelengths are displayed and also the sum intensity distribution. The advantageous behavior of the new design becomes obvious: first, no zero-order contribution is detectable and secondly the color fringe effect disappears so that a homogeneous white ring is observable. Also the cross-section of the simulated intensity (see the bottom of Figure 22) shows a significantly smaller chromatic aberration than the diffractive design (see Figure 20).

The calculated achromatic element structure was also fabricated by direct laser beam writing as a photoresist structure.

Figure 23 shows a typical section of the photoresist structure, measured by a confocal microscope. Originally, we intended to transfer this resist structure into fused silica by ion-beam etching.

Therefore, both the design and the simulation were done using refractive index and dispersion of fused silica. Because of time reasons, however, the original plan had to be changed and only the resist element could be used for experimental investigation.

Therefore, for examining the intensity distribution as measured using the resist element we will have to consider that the refractive index change of the resist material (AZ4562, Microchemicals GmbH) for the range of 480–630 nm is 5.5 times larger than that of fused silica.

The far field intensity distribution was measured using a digital photo camera and a halogen lamp as a light source. The light was collimated in order to produce a beam divergence of 5 mrad FWHM. Because of the non-uniform spectral absorption of the resist element, a yellow cast color distortion was detected. To correct this disturbing effect, the red, green, and blue (RGB) components were separated from the measured camera picture. After separation, all RGB channels were normalized and added, thus simulating a white source and equal absorption for the RGB components as found with fused silica. The upper part of Figure 24 shows the normalized RGB intensity profiles. Despite using resist with dispersion different to that of fused silica, as a first impressive result one can see that the fabricated design shows achromatic behavior in the white-light measurement.

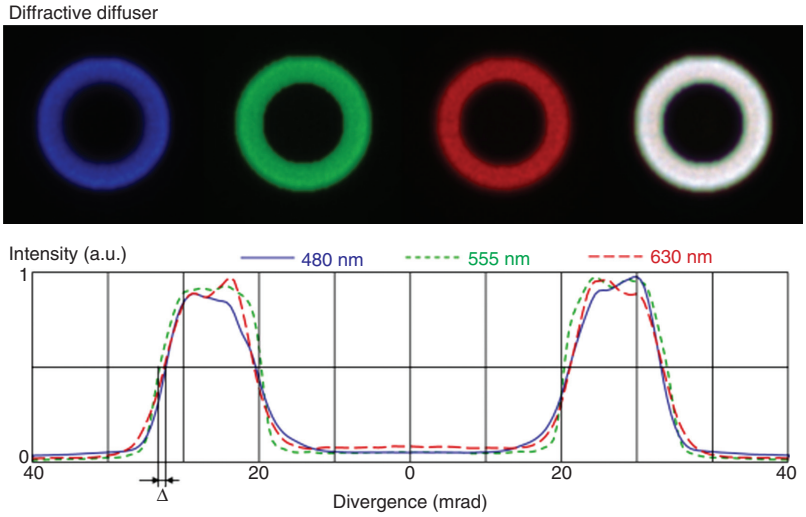

Figure 22 Top: simulated far field intensity distributions of a continuous randomized element with color correction at 480 nm, 555 nm, 630 nm (from left to right). The last ring is the addition of the RGB colors. Bottom: cross-section of simulated intensity distributions.

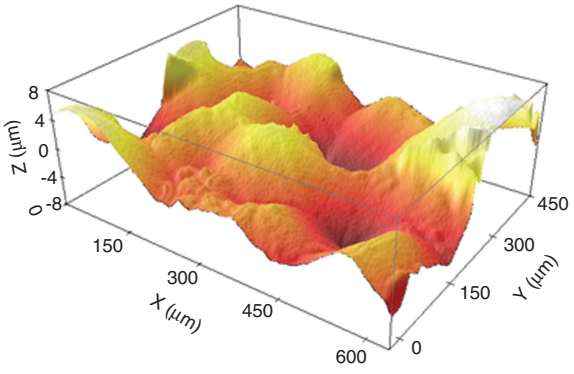

Figure 23 Confocal height measurement of the photoresist structure of an achromatic ring diffuser, measured with a confocal microscope (PLμ 2300; Sensofar; confocal mode).

Furthermore, no zero order can be detected. Nevertheless, when studied more closely, a small color mismatch can be observed. The divergence angle of the blue light profile is larger than that of the red profile. Compared to the simulated angular dispersion of the diffractive design, the achromatic design has the inverse dispersion (Figures 20 and 24). That means, in the case of the measured element configuration, we have an 'over-corrected' chromatic behavior. From the two-dimensional superposition of the RGB colors shown in Figure 25, the mentioned effect becomes obvious. Furthermore, as can be seen on top of Figure 24, the divergence of the measured ring structure is larger than the target divergence.

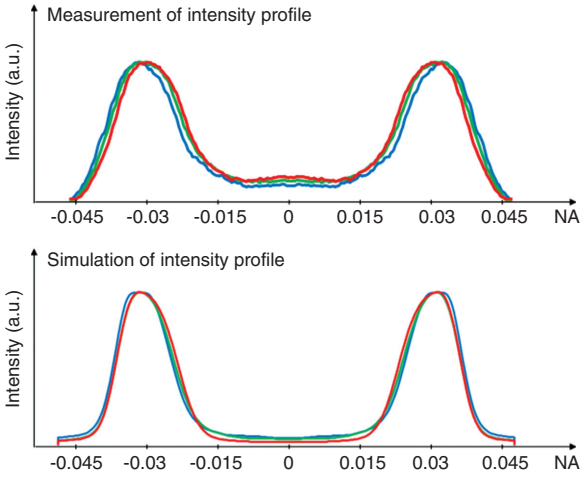

Figure 24 Far field intensity profile of a ring structure with separated RGB channels, top: measurement, bottom: simulation, taking into account the profile error and dispersion of resist material.

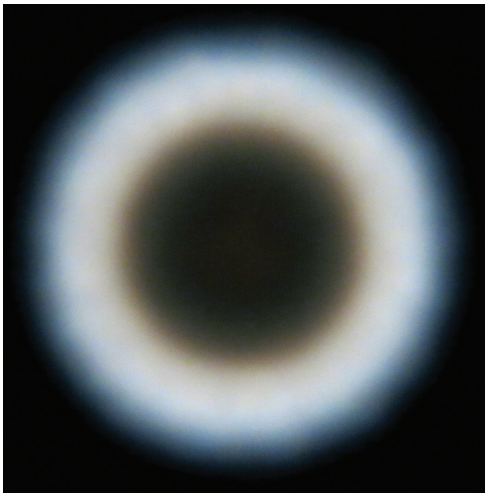

Figure 25 Photograph of the far field distribution of the achromatic corrected ring.

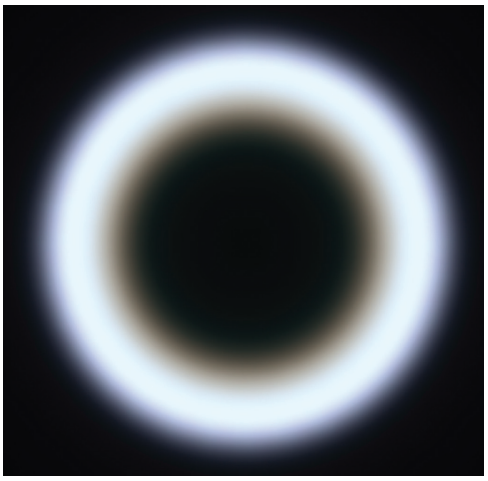

Figure 26 Simulated far field intensity distribution, taking into account the profile error and dispersion of resist material.

As mentioned above, the target center to center divergence was defined as 50 mrad. Nevertheless, the divergence measured was 64 mrad. This divergence error can be explained with a resist profile depth error factor 1/1.28 (target/measurement), which was also detected by the confocal profile measurement.

To understand the measured chromatic behavior in more detail, both the refractive index dispersion of the photoresist and the profile depth aberration were considered in a far field simulation. The simulated intensity profile (Figure 24, bottom) exhibits a chromatic distribution similar to but a little less broad than the observed one. Figure 26 shows the two-dimensional intensity distribution as obtained by the same simulation. Compared to the measured intensity profile, the simulated intensity profile has sharper edges. This suggests that very likely the divergence of the incoming white-light beam exerts a significant influence on the far field distribution.

7 Conclusion

In the present paper, the advantages of refractive micro-optical micro-lens arrays for illumination applications were discussed. To overcome disadvantageous limitations in the variety of the attainable angular distributions, a transition from regular micro-lens arrays to randomized micro-lens distributions and at the end to completely randomized, smooth, and continuous profile structures was considered. Following this way of increasing structure complexity with hard restrictions on profile continuity, an increasing potential of extended optical functionality came out. Using this potential of increased design freedom, complex angular intensity distributions without disturbing zero-order spots have been realized.

With a further extension of design freedom introducing a structure size scaling algorithm for balancing diffractive/refractive contributions of the element function, chromatic compensated designs having a homogenizing and a beam shaping functionality have been developed.

Acknowledgments: The authors would like to thank Philipp Lange for writing and measuring micro-optical elements, and Lars Erdmann and Robert Brunner for helpful and critical discussions.

References

[1] W. Singer, M. Totzeck, and H. Gross, in Handbook of Optical Systems: Physical Image Formation, Volume 2 (eds) (2005), Wiley-VCH Verlag GmbH & Co. KGaA, Weinheim, FRG. Pages 172–176, ISBN: 978-3-527-40378-3.
[2] O. Homburg, D. Hauschild, F. Kubacki and V. Lissotschenko, Proc. SPIE 6216, 621608 (2006).
[3] A. Bich, J. Rieck, C. Dumouchel, S. Roth, K. J. Weible, et al., Proc. SPIE 6879, 68790Q (2008).
[4] R. Voelkel and K. J. Weible, Proc. SPIE 7102, 71020J (2008).
[5] M. Rossi, R. E. Kunz and H. P. Herzig, Appl. Opt. 34, 5996–6007 (1995).
[6] C. Kopp, L. Ravel and P. Meyrueis, J. Opt. A: Pure Appl. Opt. 1, 398 (1999).
[7] V. Kettunen, J. Simonen, M. Kuittinen, O. Ripoll and H. P. Herzig, Diffractive elements designed to suppress unwanted zeroth order due to surface depth error, Conference Paper Diffractive Optics and Micro-Optics (DOMO, 2002). http://dx.doi.org/10.1364/DOMO.2002.DMD3.
[8] M. Cumme, P. Triebel, D. Mademann, M. Schrenk and P. Weissbrodt, Proc. SPIE 5962, 59621B (2005).
[9] M. Längle, Diffractive beam splitter, Patent DE 102007005791 A1 (2008).
[10] M. Siebold, F. Roeser, M. Loeser, D. Albach and U. Schramm, Proc. SPIE 8780, 878005 (2013).
[11] U. Vokinger, R. Dändliker, P. Blattner and H. P. Herzig, Opt. Commun. 157, 218–224 (1998).
[12] P. Ruffieux, T. Scharf, H. P. Herzig, R. Völkel and K. J. Weible, Opt. Exp. 14, 4687–4694 (2006).
[13] A. Büttner and U. D. Zeitner, Opt. Eng. 41, 2393–2401 (2002).
[14] L. H. Erdmann, A. Deparnay, F. Wirth and R. Brunner, Proc. SPIE 5347, 79 (2004).
[15] Voronoi diagram, http://en.wikipedia.org/wiki/Voronoi_diagram.
[16] R. Brunner, A. Deparnay, M. Helgert, M. Burkhardt, T. Lohmüller, et al., Proc. SPIE 7057, 705705 (2008).
[17] O. Ripoll, V. Kettunen and H. P. Herzig, Opt. Eng. 43, 2549–2556 (2004).
[18] T. R. M. Sales, Adv. Opt. Technol. 1, 127–134 (2012).
[19] D. Faklis and G. M. Morris, Appl. Opt. 34, 2462–2468 (1995).

[20] J. Néauport, X. Ribeyre, J. Daurios, D. Valla, M. Lavergne, et al., Appl. Opt. 42, 2377–2382 (2003).
[21] J. A. Marozas, J. Opt. Soc. Am. A 24, 74–83 (2007).
[22] M. M. Meyers, Catadioptric lens system incorporating diffractive achromatization, Patent US 5742431 A (1998).
[23] G. Minguez-Vega, M. Gruber, J. Jahns and J. Lancis, Appl. Opt. 44, 229–235 (2005).

Matthias Cumme
Department of Microstructured Optics, Carl Zeiss Jena GmbH, Carl Zeiss Promenade 10, 07745 Jena, Germany,
matthias.cumme@zeiss.com

Matthias Cumme received his diploma in Physics in 1998 from the Friedrich-Schiller-University in Jena, Germany. In 2008, he joined Carl Zeiss Jena GmbH. As a principal scientist he is engaged in the development of design algorithms and fabrication techniques for micro-optics.

Arnaud Deparnay
Department of Microstructured Optics, Carl Zeiss Jena GmbH, Carl Zeiss Promenade 10, 07745 Jena, Germany

Arnaud Deparnay received his diploma in Engineering Physics in 2001 from the Ecole Centrale in Marseille, France. Since 2002, he has been working as an R&D engineer for Carl Zeiss Jena GmbH. His current interests include design, fabrication, and application of micro-optics.